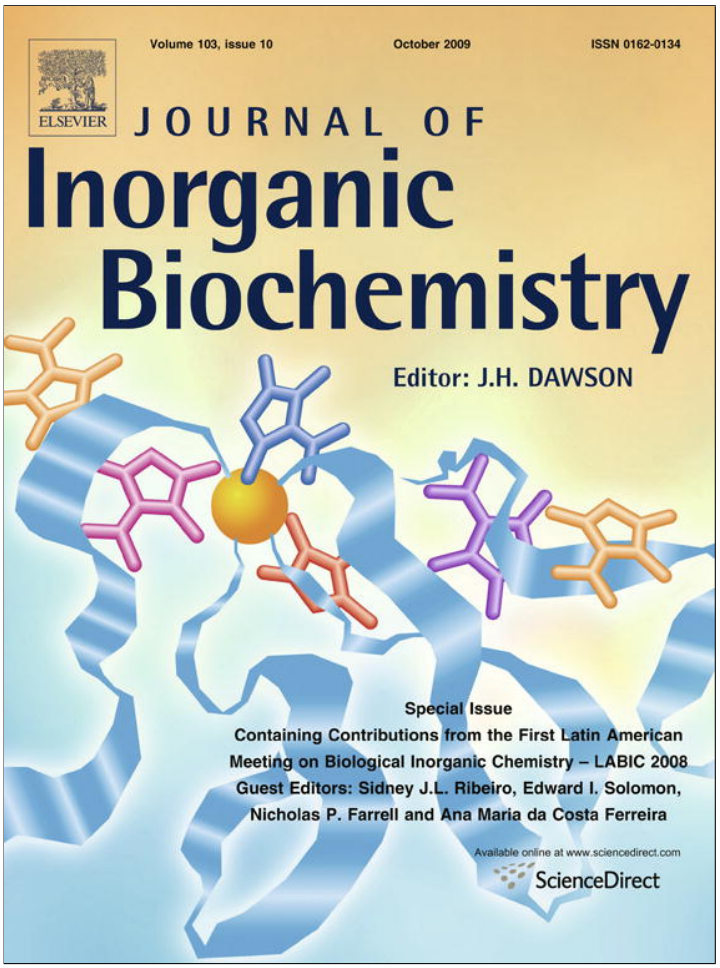

Journal of Inorganic Biochemistry 103 (2009) 1342–1346

Contents lists available at ScienceDirect

Journal of Inorganic Biochemistry

journal homepage: www.elsevier.com/locate/jinorgbio

EPR studies of the Mo-enzyme aldehyde oxidoreductase from *Desulfovibrio gigas*: An application of the Bloch–Wangsness–Redfield theory to a system containing weakly-coupled paramagnetic redox centers with different relaxation rates

Pablo J. González [a], Guillermo I. Barrera [b], Alberto C. Rizzi [b], José J.G. Moura [a], Mario C.G. Passeggi [b], Carlos D. Brondino [b,*]

[a] REQUIMTE, Departamento de Quimica, Centro de Quimica Fina e Biotecnologia, Faculdade de Ciências e Tecnologia, Universidade Nova de Lisboa, 2829–516 Caparica, Portugal
[b] Departamento de Física, Facultad de Bioquímica y Ciencias Biológicas, Universidad Nacional del Litoral, S3000ZAA Santa Fe, Argentina

ARTICLE INFO

Article history:
Received 6 May 2009
Received in revised form 19 June 2009
Accepted 22 June 2009
Available online 27 June 2009

Keywords:
Electron paramagnetic resonance
Magnetic interactions
Relaxation rate
Molybdenum-containing enzymes
Aldehyde oxidoreductase

ABSTRACT

Electron transfer proteins and redox enzymes containing paramagnetic redox centers with different relaxation rates are widespread in nature. Despite both the long distances and chemical paths connecting these centers, they can present weak magnetic couplings produced by spin–spin interactions such as dipolar and isotropic exchange. We present here a theoretical model based on the Bloch–Wangsness–Redfield theory to analyze the dependence with temperature of EPR spectra of interacting pairs of spin 1/2 centers having different relaxation rates, as is the case of the molybdenum-containing enzyme aldehyde oxidoreductase from *Desulfovibrio gigas*. We analyze the changes of the EPR spectra of the slow relaxing center (Mo(V)) induced by the faster relaxing center (FeS center). At high temperatures, when the relaxation time T_1 of the fast relaxing center is very short, the magnetic coupling between centers is averaged to zero. Conversely, at low temperatures when T_1 is longer, no modulation of the coupling between metal centers can be detected.

1. Introduction

Electron transfer proteins and redox enzymes participate in several biological processes occurring in nature [1–3]. The electron transfer chains of these proteins include distinct type of redox centers (usually situated ~10–20 Å away) connected by long chemical pathways which are thought to be involved in electron transfer processes. These centers are paramagnetic in some redox states of the proteins and, in addition, despite the long both distances and chemical paths, they can present weak magnetic couplings produced by spin–spin interactions such as dipolar and isotropic exchange, also known as superexchange interaction [4]. The strength of the dipole–dipole interaction depends mainly on the distance between centers whereas that of exchange interaction, which is characterized by the exchange interaction constant (J), on the nature of the chemical path connecting the centers, the higher the J parameter, the higher the interaction [5–8].

The fact that the redox centers in these proteins may be paramagnetic has made the Electron Paramagnetic Resonance technique a valuable tool to characterize the electronic and relaxation properties of the metal ions and the nature and magnitude of the weak magnetic coupling among centers. Particularly, the analysis of the magnetic interaction between centers by EPR can be advantageously used to determine intercenter distances, to assign the EPR active centers with those of the structure, to evaluate magnitude and nature of the magnetic coupling, and the integrity of the electron transfer pathways in distinct protein conditions [9–16]. An interesting situation occurs when the centers show different relaxation rates. When this happens, the faster relaxing center may produce a temperature dependent modulation of the magnetic couplings and an enhancement of relaxation properties of the slower relaxing center [13,16].

Mononuclear Mo-containing enzymes of the xanthine oxidase family constitute representative examples of weakly magnetic-coupled systems containing redox centers with different relaxation rates [9,12,17–20]. A common feature of these enzymes is that they contain a Mo atom in the active site and two iron–sulfur clusters of the type [2Fe–2S] called FeS 1 and FeS 2, which show intercenter magnetic couplings in certain redox potentials. Both the magnetic coupling, previously analyzed in [21], and the different relaxation rates of the interacting centers (FeS 2 > FeS 1 > Mo(V)) give rise to a temperature dependent splitting of the EPR spectra of the individual centers [22]. Although this phenomenon has been widely documented and qualitatively explained for distinct types of biological systems [13,16], to our

* Corresponding author. Fax: +54 342 4575221.
E-mail address: brondino@fbcb.unl.edu.ar (C.D. Brondino).

0162-0134/$ - see front matter © 2009 Elsevier Inc. All rights reserved.
doi:10.1016/j.jinorgbio.2009.06.006

knowledge, a theoretical model based on solid grounds that allows one to simulate the temperature dependence of EPR spectra associated with weak spin–spin interactions has never been presented.

In this paper we present a model based on the density matrix formalism as proposed by Bloch, Wangsness and Redfield (BWR) [23,24] to interpret the temperature variation of the Mo(V) EPR signals of the XO family member aldehyde oxidoreductase from *Desulfovibrio gigas* (*Dg*AOR) [25,26]. This model has been sketched previously by Salikhov et al. to analyze the reverse shift of the EPR signal of a paramagnetic center strongly-coupled by exchange to a faster relaxing species [27].[1] We extend now this model to analyze the case of a weakly-coupled pair of spin 1/2 centers (Mo and FeS 1) that in addition can show hyperfine structure at one of the centers (the Mo center). This type of studies is not only of theoretical interest but also is useful to analyze properties of this kind of systems that complement information obtained from other experimental techniques.

2. Materials and methods

*Dg*AOR was purified as described elsewhere [28,29]. Variable-temperature EPR measurements at X-band in the range 10–150 K were performed on a Bruker EMX spectrometer equipped with a dual-mode cavity (model ER 4116DM) and an Oxford Instruments continuous flow cryostat. Spectra were acquired in non-saturating conditions. Experimental conditions: microwave frequency, 9.65 GHz; modulation field, 100 kHz; modulation amplitude, 2 G; microwave power, 0.6 mW.

The temperature variation of the spectra associated with Mo(V) species was simulated using a computer program written locally based on the model described in Section 3.3 and in the Appendix given as supplementary material. The program also includes, when necessary, hyperfine coupling terms at one of the centers. The powder-like spectra were simulated assuming that all orientations of the spin pair with respect to the applied magnetic field are possible as explained in chapter 5 of Ref. [30]. The program cycles through the angles θ and ϕ systematically and calculates at each set of orientations the derivative with respect to the magnetic field of the out of phase magnetization (Eq. (4) in Section 3.3). The convolution was performed with an angular grid using m equal steps in θ and n equal steps in ϕ. The intensities of the resonance lines were corrected by the $1/g$ factor.

3. Results and discussion

3.1. Structural properties and redox cofactor organization

The structural properties of *Dg*AOR [25,26] and closely related proteins have been documented elsewhere (see Ref. [22] for a review). We present here a brief description of the structural information that is essential to analyze the EPR properties of *Dg*AOR.

*Dg*AOR is a homodimeric protein belonging to the XO family of mononuclear molybdenum-containing proteins that catalyzes the oxidation of aldehyde to acid. The X-ray data indicate that the protein crystallizes in monomeric form [25,26]. The 3D structure of each monomer is organized into two major domains called Mo-domain and FeS domain. The Mo-domain is the largest one and

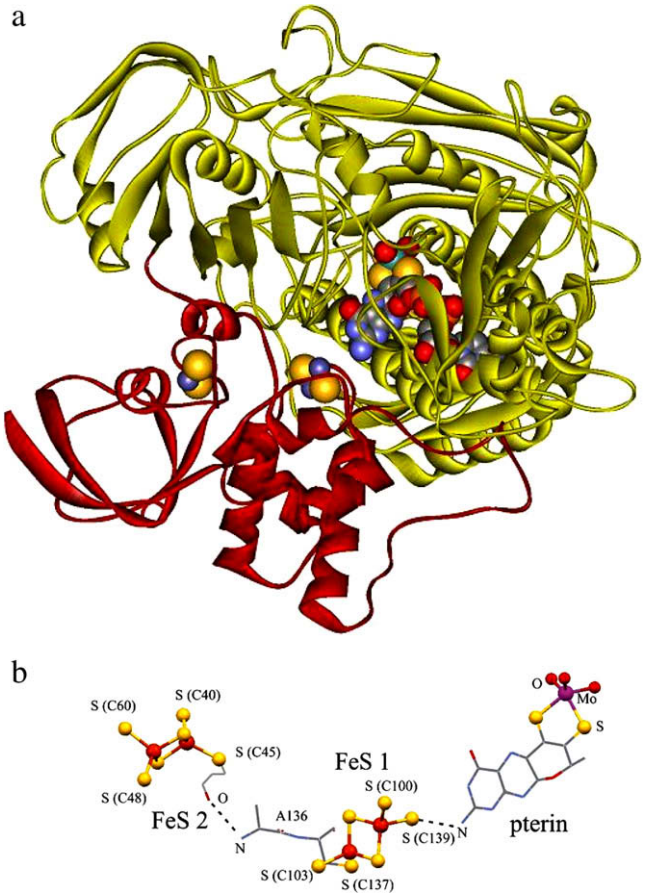

Fig. 1. (a) 3D structure of one *Dg*AOR monomer with the FeS binding domains colored in red and the Mo binding domain in yellow. (b) Proposed chemical path involved in electron transfer in *Dg*AOR.

contains the Mo active site whereas the FeS domain contains two FeS centers of the type [2Fe–2S]. Fig. 1a shows the 3D structure of one monomer in *Dg*AOR and the position of the Mo active site and both FeS clusters. The Mo atom in its oxidized form is in a distorted square pyramidal coordination with two S atoms from one pyranopterin, an oxo ligand and a OH/OH_2 molecule in equatorial positions, and an oxo ligand in the apical position (Fig. 1b). The FeS domain of *Dg*AOR can be subdivided into two subdomains, each of them containing a FeS center. One of the centers (FeS 1) is closer to the Mo site and is buried inside the protein in a helical domain inaccessible to solvent (C-terminal domain). The second cluster (FeS 2) and the corresponding domain are of the plant ferredoxin type (N-terminal domain) and are exposed to solvent. FeS 1 and FeS 2 clusters are 15 Å and 24.4 Å away, respectively, from the Mo atom. Although the X-ray structure of the protein dimer is unknown, the shortest distances between the metal cofactors and the protein monomer surface indicate that the metal centers belonging to different monomers of the same protein dimer are situated at least 40 Å away. The metal cofactors of each monomer are along an electron transfer pathway that mediates electron exchange between substrate and the electron acceptor [31]. Fig. 1b shows the proposed chemical path for electron transfer. The path connecting Mo and FeS 1 involves the pterin ligand, and a hydrogen bond involving the nitrogen and sulfur atoms from pterin and Cys139, respectively. The chemical path between FeS 1 and FeS 2 involves a mixed chemical path including the amino acids Cys137 and Ala136, which is hydrogen-bonded to the oxygen atom of Cys45.

[1] Reverse shift is an expression coined by Salikhov et al. to describe the shift of the EPR line associated with the slow relaxing center as a function of the relaxation rate of the faster relaxing center. At low relaxation rates of the faster relaxing center, the resonance line is at the gravity center of the resonance lines of the uncoupled species. When the relaxation rate increases, the resonance line shifts away from the gravity center toward the line position corresponding to the uncoupled species.

3.2. EPR properties of DgAOR

The Mo atom of the active site of *Dg*AOR can be found in three different redox states, Mo(VI), Mo(V), and Mo(IV). Of all these redox states, Mo(V) (d^1, S = 1/2) is detectable by EPR and gives rise to signals with all *g*-values lower than 2. The 2 × [2Fe−2S] centers can be obtained in two redox states. The oxidized state of both FeS clusters ($[2Fe{-}2S]^{2+}$) contains two antiferromagnetically-coupled Fe^{3+} ions with a ground state with S = 0. This redox state is diamagnetic, but becomes paramagnetic on reduction of one of the Fe^{3+} ions to Fe^{2+}. The resulting Fe^{2+}–Fe^{3+} pair is also antiferromagnetically coupled ($[2Fe{-}2S]^{1+}$, S = 1/2) [32].

Dithionite reduction of *Dg*AOR for 20 min in anaerobic conditions at a redox potential around −400 mV vs. NHE gives rise to EPR signals associated with the Mo(V) ion and the two $[2Fe{-}2S]^{1+}$ clusters (Fig. 2). The Mo(V) signal obtained under these conditions is commonly named "slow" in the literature on Mo-enzymes [2], but hereafter it will be referred as Mo(V) EPR signal. Whereas ~100% of the FeS centers are paramagnetic at this redox potential, only about 10% of the total molybdenum is obtained as Mo(V) species [29]. The Mo(V) EPR signal is detected over the whole range of temperature. The EPR signal obtained above 90 K shows a nearly axial symmetry and hyperfine structure with a species with I = 1/2 (Fig. 2, spectrum a; EPR parameters in caption to Fig. 2). The nuclear species with I = 1/2 corresponds to a solvent exchangeable proton as demonstrated from the spectrum of *Dg*AOR in ^2H_2O (Fig. 2, spectrum b). In contrast, the EPR signals of FeS 1 and FeS 2 (Fig. 2, spectra c and d; EPR parameters are given in the caption) are observed at temperatures below 80 K and 50 K, respectively, which indicates that the three centers have different spin–lattice relaxation rates (FeS 2 > FeS 1 > Mo(V)), a phenomenon characterized by the longitudinal relaxation time T_1: the longer the T_1, the smaller the relaxation rate. Changes in the relative signal amplitudes with temperature happen because of the dependence of T_1 with temperature: the higher the temperature, the shorter the T_1.

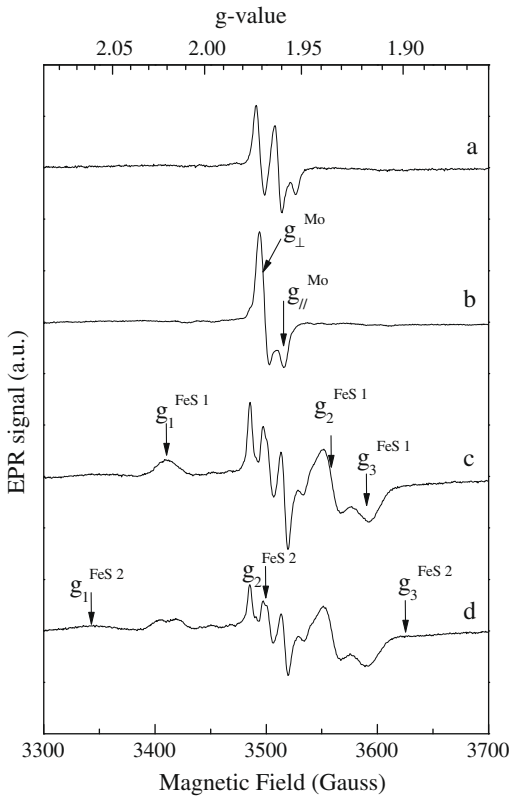

Fig. 2. EPR spectra at 100 K of *Dg*AOR in ^1H_2O (a) and ^2H_2O (b), and at 60 K (c) and 20 K (d) of *Dg*AOR in ^1H_2O. The principal *g*-values indicated with arrows on the figure are $g_1 \sim g_2 = g_{\perp} = 1.970$, $g_{\parallel} = 1.959$ for Mo(V), $g_1 = 2.023$, $g_2 = 1.938$, and $g_3 = 1.919$ for FeS 1, and $g_1 = 2.060$, $g_2 = 1.979$, and $g_3 = 1.900$ for FeS 2. The g_2 feature of FeS 2 is overlapped to the Mo(V) signal.

The spectra of Fig. 2 can be interpreted assuming two independent pairs of spin 1/2 centers, Mo(V)–FeS 1 and FeS 1–FeS 2 [9,12,21]. The Mo(V) EPR signal is split at low temperatures by FeS 1. This splitting is not observed at higher temperatures because of the high relaxation rate of FeS 1 at these temperatures. The FeS 1 signal shows splitting of its g_1 feature but by coupling with FeS 2. The FeS 1 signal splitting by Mo(V) should be also observed, but, as said above, only about 10% of the Mo–FeS 1 pair is magnetically coupled and therefore cannot be detected. In this paper we will only analyze the Mo(V)–FeS 1 pair, although a similar analysis could be also applied to the FeS 1–FeS 2 pair.

As stated in the introduction, magnetic couplings among distant redox centers in metalloproteins can originate from dipole–dipole and superexchange interactions. For an interacting spin pair, dipolar interaction splits the resonance lines of the centers in two lines whose separation depends on the magnetic field orientation with respect to the intercenter direction. In contrast, the superexchange interaction splits the resonance lines with a constant separation of $|J|$, except for those magnetic field orientations in which the difference between the effective *g*-factors (Δg) is zero, for which none or negligible splitting is observed. Furthermore, the two split lines have approximately the same intensity when $|J| < \Delta g \mu_B B$, where μ_B is the Bohr magneton, and B is the external magnetic field. If in addition, one of the centers are split by hyperfine interactions caused by species with nuclear spin (I = 1/2), it follows that this condition implies $|J| < |\Delta g \mu_B B \pm \tfrac{1}{2} A^{hfs}|$, where A^{hfs} is the hyperfine parameter. More et al. analyzed the nature of the magnetic coupling Mo(V)–FeS 1 of *Dg*AOR in ^2H_2O [21]. They found that the main features of the Mo(V) spectra can be simulated by including only the exchange interaction term ($|J| = 12 \times 10^{-4}\ cm^{-1}$) and the inclusion of dipolar terms is only necessary to correct fine details of their simulations (note that these authors used a local spin model that includes all the metal sites of the system, not the point dipole approximation). The components of the dipolar tensor in the point dipole secular approximation were estimated to be $(1.9, 1.9, -3.8) \times 10^{-4}\ cm^{-1}$ ($1\ cm^{-1} \sim 10^4$ G). The linewidth of the resonance peaks of the experimental spectra (Fig. 2) is around 9 Gauss and consequently the dipolar contribution is masked in the linewidth of the spectra. As the main objective of the present paper is to model the temperature-dependent EPR spectra of a system containing weakly-coupled paramagnetic centers with different relaxation rates, not to analyze the nature of the magnetic coupling between centers, and since the dipolar term is not relevant in this spectral simulation, it will not be considered for simplicity of the mathematical expressions. However, the extension of the model to the case of spin pairs presenting additionally anisotropic couplings is straightforward.

3.3. Theory: the basic formalism

In an EPR experiment, the basic description concerns with accounting for the response of a magnetic system in the presence of an external magnetic field, under the excitation of a radiation field. The spin Hamiltonian for an exchange-coupled spin pair in the presence of an external magnetic field B and an oscillating magnetic field b_1 is given by

$$\mathbf{H} = \mathbf{H}^S + \mathbf{H}_1^S$$

where

$$\mathbf{H}^S = \hbar\left[\omega^{(A)}S_z^{(A)} + \omega_{hfs}^{(A)}S_z^{(A)}I_z^{(A)} + \omega^{(B)}S_z^{(B)} + \omega_{exch}^{(AB)}\vec{S}^{(A)}\vec{S}^{(B)}\right] \quad (1a)$$

and, for a linearly polarized radiation field along the x direction

$$\mathbf{H}_1^S = \hbar(\omega_1^{(A)}S_x^{(A)} + \omega_1^{(B)}S_x^{(B)})\cos(\omega_o t) \quad (1b)$$

$\mathbf{H}^S$ represents the spin Hamiltonian of the system while $\mathbf{H}_1^S$ corresponds to the excitation field. The convention A = Mo(V) and B = FeS 1 is adopted for simplicity. In Eq. (1a) the first and third term represent the Zeeman interaction of the two sites A and B, respectively, both having $S^{(A)} = S^{(B)} = 1/2$, with the external magnetic field ($\omega^{(K)} = g^{(K)}\mu_B B/\hbar$). The second term corresponds to the hyperfine interaction at site A and the last term gives the Heisenberg exchange between the spins of both sites ($\omega_{exch}^{(AB)} = J/\hbar$). In Eq. (1b) $\omega_1^{(K)} = g^{(K)}\mu_B b_1/\hbar$ and ω_o are the field and excitation frequency, respectively.

The response signal can be obtained from the mean value of the out of phase magnetization [27],

$$\langle M_y\rangle \equiv -\frac{\hbar}{b_1}\sum_{m_I} Tr\left\{(\omega_1^{(A)}S_y^{(A)} + \omega_1^{(B)}S_y^{(B)})\boldsymbol{\sigma}(t, m_I)\right\} \quad (2)$$

where $\boldsymbol{\sigma}(t, m_I)$ represents the density matrix operator for the spin system, in which m_I is the projection of the nuclear spin I interacting with $S^{(A)}$. The matrix elements of this operator are calculated keeping only the right component of the two counter circularly polarized excitations in which the linearly polarized $\mathbf{H}_1^S$ can be decomposed. The matrix elements of the operator $\boldsymbol{\sigma}(t, m_I)$ accounting for the relaxation processes of the spin pair can be obtained from the BWR formulation [24] and the detailed procedure to determine its elements is in an Appendix given as supplementary material. After some well known although lengthy calculation, one arrives to a system of equations to be solved for the $\boldsymbol{\sigma}$'s, which in matrix form can be written as [27]

$$\mathbf{C}(m_I)\boldsymbol{\sigma}_R(m_I) = \mathbf{A}(m_I) \quad (3)$$

Matrix $\mathbf{C}(m_I)$ involves in addition to the Hamiltonian parameters of Eqs. (1a) and (1b), the relaxation rates of each center, matrix $\mathbf{A}$ involves the microwave frequency and equilibrium density matrix elements, while matrix $\boldsymbol{\sigma}_R(m_I)$ correspond to $\boldsymbol{\sigma}(t, m_I)$ in the stationary regime approximation in the rotating system. The explicit forms of these matrixes are given in the Appendix.

The solution of Eq. (3) using the basis states $\{|\Psi_i(m_I)\rangle\}$ given explicitly in the Appendix and the ladder operators $S_y^{(A,B)} = \frac{1}{2i}(S_+^{(A,B)} - S_-^{(A,B)})$, as well as the Hermitian properties of the elements of the density matrix ($\boldsymbol{\sigma}_{i,j} = \boldsymbol{\sigma}_{j,i}^*$), allows one to write Eq. (2) as

$$\langle M_y\rangle \equiv \frac{\hbar}{b_1}\sum_{m_I}\mathrm{Im}\{\omega_1^{(A)}[\boldsymbol{\sigma}_{R13}(m_I) + \boldsymbol{\sigma}_{R24}(m_I)] + \omega_1^{(B)}[\boldsymbol{\sigma}_{R12}(m_I) + \boldsymbol{\sigma}_{R34}(m_I)]\} \quad (4)$$

The simulated spectra were obtained by convoluting (see Section 2) the derivative of this equation with respect to the magnetic field. For the present case the matrix of Eq. (3) can be solved analytically, although it leads to a set of cumbersome expressions which, with exceptions for some limiting cases, can be more advantageously analyzed with the help of numerical methods.

It is important to note that in the case of no coupling ($\omega_{exch}^{(AB)} = 0$), Eq. (4) predicts two independent spectra with positions $\omega^{(K)} = g^{(K)}\mu_B B/\hbar$ ($K = A$ or B) associated with spins resonating independently according to Bloch equations in non-saturating conditions (see demonstration in the Appendix). The relaxation time T_2 that determines the linewidth for the EPR transitions of each spin (see Appendix) can be written as

$$\frac{1}{T_2^{A(B)}} = \frac{1}{2T_1^{A(B)}} + \frac{1}{T_{2'}^{A(B)}} \quad (5)$$

where we are assuming that $T_1^{A(B)}$ and $T_{2'}^{A(B)}$ correspond to the spin–lattice and spin–spin relaxation times, respectively.

3.4. Analysis of the EPR data

Left panels of Fig. 3 show in detail the temperature dependence of the Mo(V) EPR signal of *Dg*AOR in ^1H_2O (upper) and ^2H_2O (bottom). The right panels of Fig. 3 correspond to simulations obtained with Eq. (4) at different relaxation times T_1 of the fast relaxing center (FeS 1 or B in our nomenclature) assuming that the condition $|J|/\hbar < |\omega^{(A)} - \omega^{(B)}|$ is fulfilled for all the magnetic field orientations with respect to the spin pair molecular frame. The best agreement between experiment and simulation was obtained with an exchange parameter $|J| = 1.2 \times 10^{-3}$ cm^{-1}. The same value was reported by More et al. and was associated with the chemical path between the Mo atom and the FeS 1 center (Fig. 1b) [21]. The remaining parameters used in the simulation are given in the caption to Fig. 3. It is important to note that the relaxation times T_1 used for simulation show good agreement with those determined for FeS 1 in reference [12]. The linewidth used for simulation is given by $\frac{1}{T_2^A}$ in field units (Eq. (5)). The fact that the T_2 for Mo(V) ion is temperature independent indicates that T_1^A is very long in the range 20–150 K, i.e. its contribution to the linewidth can be neglected when compared to that of $T_{2'}^A$. In our simulations we

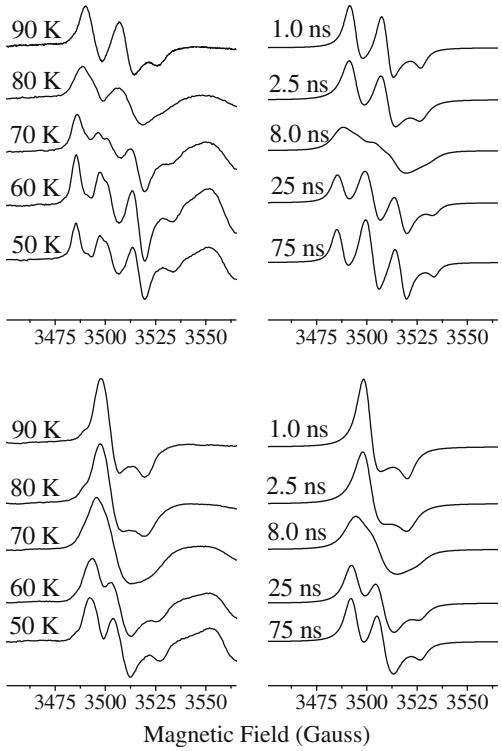

Fig. 3. Experimental Mo(V) EPR signals of *Dg*AOR (left panel) together with simulation (right panel). The top and bottom panels correspond to samples in ^1H_2O and ^2H_2O, respectively. Temperatures of the experiment and relaxation times for simulation are indicated. The spin Hamiltonian parameter for simulation of Mo(V) signals in ^2H_2O were $g_1 = 1.971$ (4), $g_2 = 1.969$ (4), and $g_3 = 1.959$ (4) and $|J| = 1.2 \times 10^{-3}$ cm^{-1}. The values in parenthesis correspond to the linewidth in Gauss. Same parameters and $A_1^{hfs} = 15$ Gauss, and $A_2^{hfs} = A_3^{hfs} = 16$ Gauss (hyperfine tensor of the solvent exchangeable proton) except the linewidths (2.5, 2.5, 2.5) were used for the sample in ^1H_2O. g- and A^{hfs}-tensors were assumed to be collinear. For *Dg*AOR in ^2H_2O, the ^2H hyperfine splitting is not considered explicitly but is folded into the linewidth.

are assuming that $\frac{1}{T_2^A}$ includes all contributions to the linewidth (homogenous and inhomogeneous). For *Dg*AOR in ^1H_2O, $\frac{1}{T_2^A}$ determines the linewidth of each hyperfine component m_I. For *Dg*AOR in ^2H_2O, $\frac{1}{T_2^A}$ includes the unsolved deuterium hyperfine structure, as the simulation was performed assuming a Mo(V) ion with no hyperfine structure due to ^2H. Similar assumption was made by other authors to analyze chemical exchange processes by generalized Bloch equations [33].

By inspecting Fig. 3, two well differentiated regimes can be clearly identified at both extremes of the temperature range. At high temperature ($T \geqslant 90$ K), when spin *B* (FeS 1) relaxes extremely fast so that it has a very short relaxation time ($T_1^{FeS\ 1} \leqslant 1$ ns), Eq. (4) predicts Mo(V) spectra corresponding to those of an uncoupled system. This means that the fast relaxing center is modulating the interaction between centers in such a way that the effect of the spin coupling is averaged to zero. In contrast, at low temperatures ($T \leqslant 50$ K) when FeS 1 center relaxes slow ($T_1^{FeS\ 1} \geqslant 75$ ns), no modulation of the spin coupling can be detected, and the spectra correspond to those of the coupled system. Intermediate situations with partial collapse and broadening of the Mo(V) resonances are observed between these two limits.

Interacting magnetic centers showing temperature-dependent EPR spectra have been analyzed in terms of the generalized Bloch equations, in which the two spins *A* and *B*, which resonate at different frequencies, transform themselves with a rate $\frac{1}{\tau} = \frac{1}{\tau_A} + \frac{1}{\tau_B}$, where $1/\tau_A$ and $1/\tau_B$ are the rates of each center [33]. These equations have been used, for example, to assign the EPR signal of the proximal iron–sulfur cluster to the Mo(V) ion in the XO family [12] and to evaluate the relaxation time T_1 of the fast relaxing center in metal-nitroxyl coupled systems [34]. The central assumptions of these works is that T_1 of the fast relaxing center is associated with τ and that the splitting of the slow relaxing center at low temperatures corresponds to $\omega^{(A)} - \omega^{(B)}$. Although these assumptions give good description of the experimental data, the application of generalized Bloch equations for weakly exchange coupled systems is unjustified from a theoretical point of view. First, no chemical exchange is present between the interacting centers *A* and *B*. Second, in the absence of chemical exchange ($\frac{1}{\tau} = \frac{1}{T_1^{(B)}} \to 0$), generalized Bloch equations reduce to two magnetically uncoupled species (no splitting should be observed for each center), which clearly is not the case analyzed in this paper. Third, generalized Bloch equations are a simpler case of more general theories developed to explain EPR spectra of extended exchange coupled systems, in which $\frac{1}{\tau}$ corresponds to $\omega_{exch}^{(AB)} = J/\hbar$ [4,35,36], but not for the case of an isolated exchange-coupled spin pair.

The good agreement between experiment and simulation confirms the robustness of the BWR model to fully analyze EPR spectra of spin pairs presenting temperature dependent weak or strong magnetic couplings. The first direct application that emerges is that this model can be used to determine relaxation rates of the fast relaxing center in weakly-coupled spin pairs. Furthermore, it constitutes a powerful tool to assign the metal centers detected by EPR spectroscopy with those observed in the X-ray structure in systems containing three or more paramagnetic centers. We demonstrate here that the problem of the center assignment, which has been the subject of long debates in the proteins belonging to the XO family [22], can be precisely solved through this model.

4. Abbreviations

Xanthine oxidase XO
Iron–sulfur cluster FeS
Bloch, Wansgness and Redfield BWR
*Dg*AOR aldehyde oxidoreductase from *Desulfovibrio gigas*

Acknowledgments

P.J.G. thank Fundação para a Ciência e Tecnologia for funding (Grant SFRH/BPD/29812/2006). C.D.B. and J.J.G.M. thank SECYT (Argentina) and GRICES (Portugal) for a bilateral collaborative grant. Work supported by projects, POCTI/QUI/57701/2004 in Portugal, and SEPCyT:PICT 2006-00439, CONICET PIP 112-200801-01079 and CAI+D-UNL in Argentina. C.D.B is member of CONICET (Argentina).

Appendix A. Supplementary material

An Appendix describing the procedure to determine the elements of the density matrix operator accounting for the relaxation processes of a spin pair through the BWR formulation is provided as Supplementary data. Supplementary data associated with this article can be found, in the online version, at doi:10.1016/j.jinorgbio.2009.06.006.

References

[1] W.G. Zumft, Microbiol. Mol. Biol. Rev. 61 (1997) 533–616.
[2] R. Hille, Chem. Rev. 96 (1996) 2757–2816.
[3] H.B. Gray, J.R. Winkler, Annu. Rev. Biochem. 65 (1996) 537–561.
[4] A. Bencini, D. Gatteschi, Electron Paramagnetic Resonance of Exchange Coupled Systems, Springer-Verlag, Berlin, 1990.
[5] O. Kahn, Angew. Chem. Int. Ed. Engl. 24 (1985) 834–850.
[6] S.K. Hoffmann, W. Hilczer, J. Goslar, Appl. Magn. Reson. 7 (1994) 289–321.
[7] J.M. Schveigkardt, A.C. Rizzi, O.E. Piro, E.E. Castellano, R. Costa de Santana, R. Calvo, C.D. Brondino, Eur. J. Inorg. Chem. (2002) 2913–2919.
[8] A.C. Rizzi, C.D. Brondino, R. Calvo, R. Baggio, M.T. Garland, R.E. Rapp, Inorg. Chem. 42 (2003) 4409–4416.
[9] S.L. Andrade, C.D. Brondino, M.J. Feio, I. Moura, J.J. Moura, Eur. J. Biochem. 267 (2000) 2054–2061.
[10] A. Thapper, D.R. Boer, C.D. Brondino, J.J. Moura, M.J. Romao, J. Biol. Inorg. Chem. 12 (2007) 353–366.
[11] R. Calvo, M.C. Passeggi, R.A. Isaacson, M.Y. Okamura, G. Feher, Biophys. J. 58 (1990) 149–165.
[12] J. Caldeira, V. Belle, M. Asso, B. Guigliarelli, I. Moura, J.J. Moura, P. Bertrand, Biochemistry 39 (2000) 2700–2707.
[13] S.S. Eaton, G.R. Eaton, Coordin. Chem. Rev. 83 (1988) 29–72.
[14] D.J. Hirsh, W.F. Beck, J.B. Innes, G.W. Brudvig, Biochemistry 31 (1992) 532–541.
[15] D.J. Hirsh, W.F. Beck, J.B. Lynch, L. Que, G.W. Brudvig, J. Am. Chem. Soc. 114 (1992) 7475–7481.
[16] S.S. Eaton, G.R. Eaton, Coordin. Chem. Rev. 26 (1978) 207–262.
[17] D.J. Lowe, R.M. Lynden-Bell, R.C. Bray, Biochem. J. 130 (1972) 239–249.
[18] A. Thapper, M.G. Rivas, C.D. Brondino, B. Ollivier, G. Fauque, I. Moura, J.J. Moura, J. Inorg. Biochem. 100 (2006) 44–50.
[19] C. Canne, D.J. Lowe, S. Fetzner, B. Adams, A.T. Smith, R. Kappl, R.C. Bray, J. Huttermann, Biochemistry 38 (1999) 14077–14087.
[20] M. Boll, G. Fuchs, C. Meier, A. Trautwein, A. El Kasmi, S.W. Ragsdale, G. Buchanan, D.J. Lowe, J. Biol. Chem. 276 (2001) 47853–47862.
[21] C. More, M. Asso, G. Roger, B. Guigliarelli, J. Caldeira, J. Moura, P. Bertrand, Biochemistry 44 (2005) 11628–11635.
[22] C.D. Brondino, M.J. Romao, I. Moura, J.J. Moura, Curr. Opin. Chem. Biol. 10 (2006) 109–114.
[23] C.P. Slichter, Principles of Magnetic Resonance, Springer-Verlag, New York, 1990.
[24] N.M. Atherton, Electron Spin Resonance; Theory and Applications, E. Horwood Ltd., Chichester, 1973.
[25] M.J. Romao, M. Archer, I. Moura, J.J. Moura, J. LeGall, R. Engh, M. Schneider, P. Hof, R. Huber, Science 270 (1995) 1170–1176.
[26] J.M. Rebelo, J.M. Dias, R. Huber, J.J. Moura, M.J. Romao, J. Biol. Inorg. Chem. 6 (2001) 791–800.
[27] K.M. Salikhov, R.T. Galeev, V.K. Voronkova, Y.V. Yablokov, J. Legendziewicz, Appl. Magn. Reson. 14 (1998) 457–472.
[28] J.J. Moura, A.V. Xavier, M. Bruschi, J. Le Gall, D.O. Hall, R. Cammack, Biochem. Biophys. Res. Commun. 72 (1976) 782–789.
[29] J.J. Moura, A.V. Xavier, R. Cammack, D.O. Hall, M. Bruschi, J. Le Gall, Biochem. J. 173 (1978) 419–425.
[30] J.R. Pilbrow, Transition Ion Electron Paramagnetic Resonance, Oxford University Press, New York, 1990.
[31] C.D. Brondino, M.G. Rivas, M.J. Romao, J.J. Moura, I. Moura, Acc. Chem. Res. 39 (2006) 788–796.
[32] M.K. Johnson, Curr. Opin. Chem. Biol. 2 (1998) 173–181.
[33] H.S. Gutowsky, C.H. Holm, J. Chem. Phys. 25 (1956) 1228–1234.
[34] L. Fielding, K.M. More, G.R. Eaton, S.S. Eaton, J. Am. Chem. Soc. 108 (1986) 8194–8196.
[35] D.M. Martino, M.C.G. Passeggi, R. Calvo, Phys. Rev. B 52 (1995) 9466–9476.
[36] S.K. Hoffmann, Chem. Phys. Lett. 98 (1983) 329–332.